Multi-Modal Elderly Monitoring via Wearable Devices and WiFi-Enabled Edge-Cloud Architecture with HRV-Based Fall Detection

Cui Huang[1], Runguo Chai[2*]
[1]Department of Rehabilitation Therapy, Langfang Health Vocational College, Langfang, 065001, China
[2]Department of Nursing, Langfang Health Vocational College, Langfang, 065001, China
E-mail: chrg_crg@outlook.com
[*]Corresponding author

Keywords: wearable monitoring, WiFi, HRV, Fall detection, multi-modal fusion

Received: September 11, 2025

In elderly health monitoring scenarios, events such as falls and cardiac arrhythmias are often sudden and high-risk, making traditional single-indicator monitoring methods insufficient for real-time and accurate detection in complex environments. To enhance system stability and anomaly detection capability under multi-interference conditions, this study develops a wearable monitoring system based on WiFi communication technology. The system integrates physiological signal acquisition, environmental parameter sensing, and dynamic threshold and weight adjustment mechanisms, achieving low-latency and high-reliability data processing and alert response within an edge-cloud collaborative architecture. Experiments were conducted using the SisFall Dataset and the MIT-BIH Physiological Signal Database. The K-Nearest Neighbors (KNN) classifier is employed for anomaly detection. The results showed that under optimal parameter configuration, the system achieved a maximum F1-score of 0.94, peak sensitivity of 94.8%, minimum event detection latency of 140 ms, and a minimum false alarm rate of only 3.8%. The simulation tests further verify the robustness and adaptability of the system under low, medium, and high interference environments, demonstrating its feasibility for deployment in smart elderly care and remote healthcare applications.

Povzetek: Prispevek predstavi nosljiv sistem za spremljanje zdravja starejših, ki z WiFi povezavo in prilagodljivim zaznavanjem anomalij omogoča hitro in zanesljivo odkrivanje padcev ter srčnih motenj tudi v zahtevnih okoljih.

1 Overview

In recent years, the world has entered an aging stage. The United Nations predicts that by 2050, the population aged 60 and above will account for over 22% of the total global population, with a significant proportion being elderly people living alone or empty nesters [1]. For this group, issues such as chronic diseases, sudden illnesses, and frequent falls not only seriously affect their quality of life, but may also cause irreversible consequences in the absence of timely assistance [2]. The traditional passive alarm method is difficult to meet the all-weather and real-time monitoring needs, so there is an urgent need to use intelligent and automated technological means to make up for this deficiency. With the integration of artificial intelligence and the medical field, medical monitoring devices equipped with artificial intelligence technology have gradually become mainstream in the market [3]. Wearable devices have become one of the important solutions for elderly health monitoring due to their miniaturization, low power consumption, and non-invasiveness. Babu et al. proposed a wearable device that integrated physical, chemical, and biological sensors, which enables non-invasive and continuous monitoring of vital signs. The research results have promoted the early detection and precise management of wearable devices in multiple fields such as cardiovascular disease, viral infections, and mental health [4]. Dewangan et al. designed an energy-saving intelligent wearable device to address the serious injuries and delayed rescue in elderly people who fall. This device monitored human fall behavior through sensors and combined ESP8266-01 chip to achieve cloud data transmission and emergency assistance, improving the response efficiency of elderly fall incidents [5]. Tan et al. designed a wearable cardiovascular monitoring device based on 5G and deep learning to solve the problem that COVID-19 patients were often accompanied by cardiovascular diseases and lack of efficient real-time monitoring. The experimental results showed that the device could improve the accuracy of cardiovascular disease prediction to 99.29%, effectively solving the high communication latency and manual diagnosis dependence in traditional methods [6].

However, to maximize the performance of wearable devices, it is necessary to rely on stable and efficient data transmission channels to quickly transmit multi-modal data collected at the edge to the cloud or collaborative nodes for processing. Among various wireless

communication methods, WiFi demonstrates unique adaptability in home and community monitoring scenarios due to its high bandwidth, wide coverage, and high device popularity [7]. In recent years, researchers have achieved multiple results in intelligent monitoring systems based on WiFi communication. He J et al. proposed a non-contact fall detection method based on channel state information of commercial WiFi devices to address the weak cross-scenario adaptability of traditional fall detection systems. The experimental results on the test dataset showed that the method could still maintain a detection accuracy of over 95.25% even under environmental changes [8]. Ghoshal et al. reviewed existing indoor positioning research and tested various WiFi fingerprint positioning algorithms on self-built datasets, focusing on the important role of indoor positioning in medical scenarios in the Internet of Things environment. The floor recognition rates of various algorithms were all above 90%, verifying the potential application of WiFi fingerprint positioning models in indoor navigation, emergency response, and smart infrastructure [9]. Zhang et al. designed a contactless vital sign monitoring system based on low-cost commercial WiFi devices to address the continuous monitoring and non-invasive needs of sleep patients for vital signs. The system accurately captured respiration and heartbeat through non line of sight signal modeling and motion pattern segmentation methods. The experimental results showed good sensitivity and accuracy in vital sign monitoring, verifying the practicality and reliability of the WiFi-based contactless monitoring system in continuous health monitoring [10].

In summary, wearable monitoring systems integrating WiFi communication have shown strong adaptability and development potential in elderly care applications, yet several limitations remain. Existing studies often focus on single physiological indicators or isolated abnormal events, lacking multi-source data fusion and dynamic weighting mechanisms, which restricts comprehensive health assessment. To address these issues, this work fuses WiFi communication information with multi-modal wearable sensing data to develop an intelligent monitoring system featuring dynamic threshold adjustment and multi-path fault-tolerant decision-making. This study aims to jointly model physiological, motion, and environmental data, while improving real-time performance and computational efficiency through on-device data fusion and lightweight edge inference. It is hypothesized that multi-modal feature fusion and dynamic alert mechanisms can significantly enhance detection accuracy and stability, while WiFi optimization and compression-compensation mechanisms can effectively reduce latency and strengthen transmission robustness. Under low-latency and high-reliability conditions, the proposed system demonstrates adaptability to complex environments, providing a scalable and highly innovative solution for smart elderly care and remote healthcare applications.

2 Materials and methods

2.1 Construction of wearable device monitoring system based on WiFi communication

To achieve real-time monitoring and efficient transmission of multidimensional health status of the elderly, a multi-modal wearable elderly monitoring model based on WiFi communication technology is developed. The model integrates functional modules such as physiological signal acquisition, environmental parameter monitoring, WiFi data transmission, and cloud analysis, and achieves low latency and high reliability data processing and abnormal alarm through cloud-edge-end collaborative architecture. Wearable terminals are the core of data acquisition and preliminary processing, and their hardware module composition is shown in Figure 1.

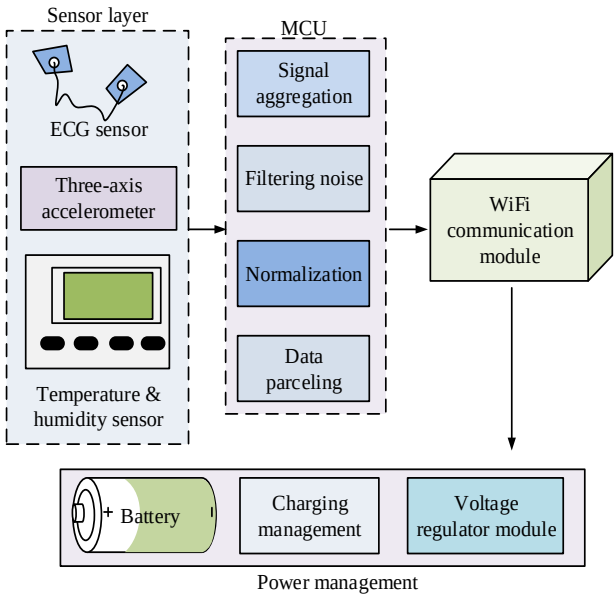

Figure 1: Hardware module composition of the wearable terminal

As shown in Figure 1, wearable terminals are composed of multiple types of sensors, Microcontroller Units (MCUs), power management modules, and WiFi communication modules. Electrocardiogram (ECG) sensors can continuously acquire ECG signals, three-axis accelerometers are used to obtain human motion status information, and temperature and humidity sensors monitor living environment parameters [11-12]. The MCU is responsible for aggregating and preprocessing multi-source signals, and real-time communication with edge nodes through low-power WiFi modules [13]. The power management module ensures stable operation of the device under long-term wearing conditions, improving the comfort and reliability of daily use for the elderly. In the signal acquisition stage, the ECG signal first passes through a bandpass filter to remove power frequency interference and baseline drift, as shown in equation (1) [14].

$$S_{ECG}(t) = F_{bp}(x(t), f_1, f_h) \quad (1)$$

In equation (1), $x(t)$ represents the original ECG signal. $S_{ECG}(t)$ represents the signal processed by bandpass filtering. t represents the sampling time of the signal. F_{bp} represents the bandpass filter operator. f_1 and f_h represent the low-frequency and high-frequency cutoff frequencies of the filter, respectively. To suppress baseline drift and high-frequency noise, a fourth-order Butterworth IIR bandpass filter with cut-off frequencies of 0.5 Hz and 50 Hz is applied, which effectively retains the primary physiological components such as QRS complexes. The filtering is implemented using the SciPy signal processing library in Python, with mirror padding at signal boundaries to minimize phase distortion. The composite acceleration value of three-axis acceleration in motion state assessment is shown in equation (2).

$$A(t) = \sqrt{a_x^2(t) + a_y^2(t) + a_z^2(t)} \quad (2)$$

In equation (2), $a_x(t)$, $a_y(t)$, and $a_z(t)$ represent the acceleration components in the three directions of x, y, and z, respectively. $A(t)$ represents the synthetic acceleration, used for fall detection and activity pattern recognition. Environmental parameters need to be normalized before transmission to ensure comparability of features with different dimensions. The normalization is shown in equation (3).

$$E_{norm}(i) = \frac{E_i - E_{min}}{E_{max} - E_{min}} \quad (3)$$

In equation (3), E_i represents the environmental parameter value of the i-th sampling point. E_{min} and E_{max} represent the minimum and maximum values of the parameter, respectively. $E_{norm}(i)$ represents the normalized environmental parameter value. After completing the collection and preprocessing, the data is transmitted to the edge or cloud for analysis through a WiFi link, as shown in Figure 2.

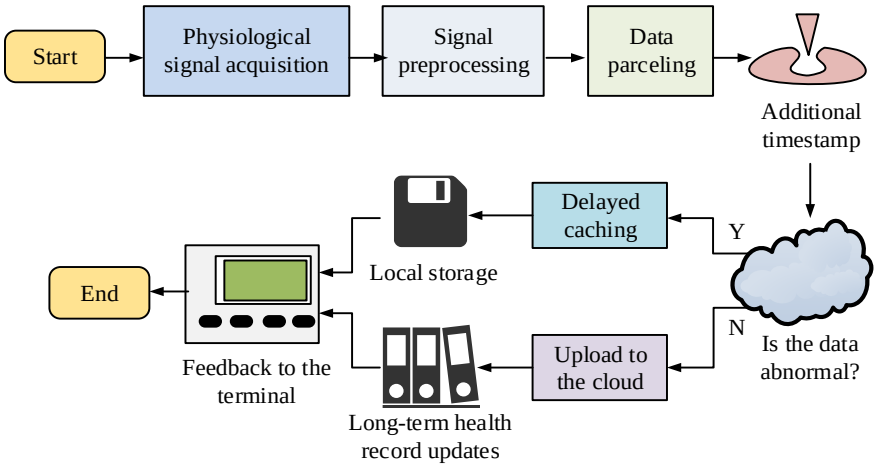

Figure 2: Data acquisition and WiFi transmission process

As shown in Figure 2, the entire data collection and WiFi transmission process is carried out in chronological order. Firstly, wearable terminals collect multi-source signals and perform preprocessing operations such as filtering, denoising, and normalization on the original signals to ensure the stability and consistency of the input data. Secondly, the MCU divides the preprocessed data into packets and adds timestamps, and sends the data to the edge nodes through the WiFi module. Edge nodes quickly analyze the received data to determine if there are any abnormal events. When the detection result is abnormal, the data will be prioritized for reporting to the cloud for in-depth analysis. When the detection result is normal, the data will enter the latency cache or be synchronized to the cloud according to the set cycle to reduce network bandwidth usage [15]. Finally, after completing the multi-modal fusion analysis, the cloud will return the monitoring results and alarm information to the terminal, achieving local prompts or emergency alarms. The WiFi link quality can be estimated by the received signal strength indicator to determine the transmission distance, as shown in equation (4).

$$d = 10^{\frac{P_t - P_r - L_0}{10n}} \quad (4)$$

In equation (4), P_t and P_r represent the signal strength at the transmitting and receiving ends, respectively. L_0 represents the reference distance path loss. n represents the path loss index. d represents the estimated transmission distance. In anomaly detection, an adjustable hyperparameter α_1 is introduced to set a dynamic warning threshold, as shown in equation (5).

$$\delta(t) = \begin{cases} 1, V(t) \geq \alpha \cdot \mu V \\ 0, \text{otherwise} \end{cases} \quad (5)$$

In equation (5), $V(t)$ represents the monitoring value

of a single tube. μV represents the mean under normal conditions. α represents the adjustment coefficient of the warning threshold. $\delta(t)$ represents the warning signal flag. When the value is 1, it indicates triggering the warning. When the value is 0, it indicates not triggering. The total latency of the system is composed of collection latency, transmission latency, and processing latency, as shown in equation (6).

$$T_{total} = T_{acq} + T_{tx} + T_{proc} \quad (6)$$

In equation (6), T_{acq} represents the acquisition latency. T_{tx} represents WiFi transmission latency. T_{proc} represents the processing latency at the edge or in the cloud. T_{total} represents the overall latency of the system. After combining hardware modules, data collection and transmission processes, and cloud-edge-end collaborative mechanisms, a complete overall architecture is formed, as shown in Figure 3.

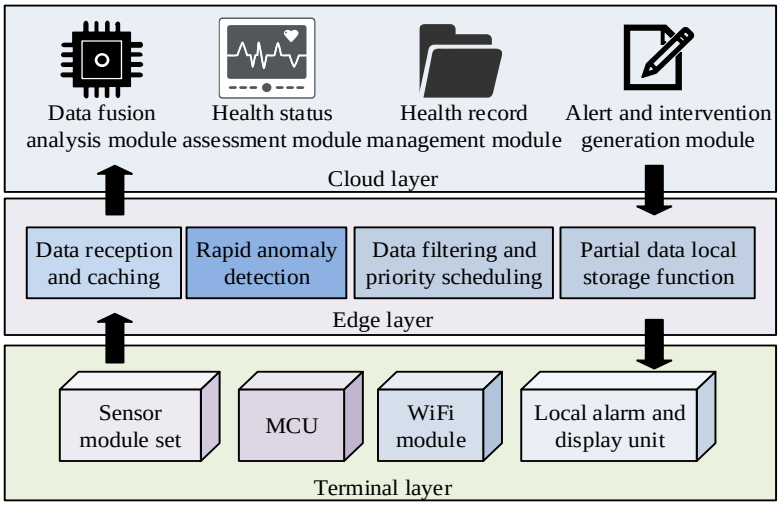

Figure 3: Overall architecture of the wearable elderly monitoring

As shown in Figure 3, the overall architecture of the monitoring system is divided into three parts: terminal layer, edge layer, and cloud layer. The terminal layer is responsible for real-time data collection and preliminary processing, including multiple types of sensor modules, data processing units, and WiFi communication modules. It is also equipped with local alarm and display functions to directly alert users in emergency situations. The edge layer is responsible for data reception and rapid screening, and can immediately perform lightweight anomaly detection upon receiving data, and prioritize scheduling based on the importance and urgency of the data. The cloud layer performs multi-modal data fusion analysis and long-term health record management, utilizing the combination of historical and real-time data to achieve accurate health status assessment and prediction, and generating personalized warning and intervention plans. The results are then fed back to the edge and terminal layers to ensure that the monitoring system can maintain stable and efficient operation under different network conditions.

2.2 Performance optimization of wearable monitoring system based on multi-modal fusion and dynamic weighting

After constructing a wearable device monitoring system based on WiFi communication, to further improve the data transmission stability and anomaly detection accuracy in complex home environments, the research introduces data compression and batch transmission mechanisms, multi-modal fusion algorithms, and dynamic threshold and weight adjustment methods [16-17]. The basic framework of this optimization method is shown in Figure 4.

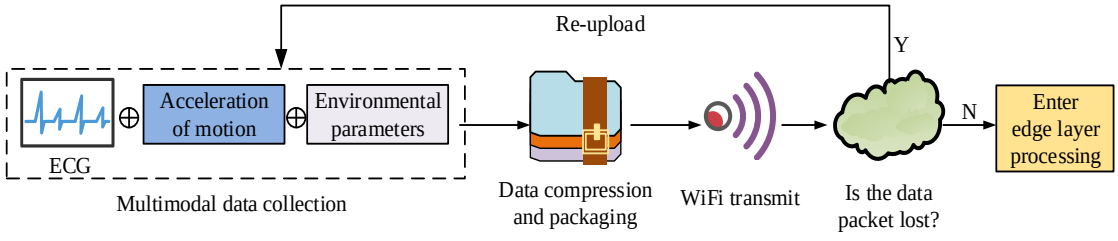

Figure 4: WiFi Transmission optimization and packet loss compensation flow

As shown in Figure 4, the WiFi transmission optimization and packet loss compensation flow introduces several improvements to the original system. Firstly, after completing data acquisition and preprocessing, the terminal compresses and batches the data to reduce transmission frequency and network load. During WiFi transmission, the system continuously monitors link quality and packet loss, automatically triggering re-transmission for missing or corrupted packets to ensure data integrity. When receiving data, the edge node prioritizes abnormal events and dynamically adjusts the alert threshold and feature weighting according to variations in real-time Signal-to-Noise Ratio (SNR), signal fluctuation amplitude, and packet loss rate. This adaptive mechanism allows the system to maintain detection stability and sensitivity under changing environmental conditions. When signal quality degrades or noise increases, the threshold is raised to suppress false alarms. Under stable conditions, it is lowered to enhance responsiveness. The adjustment logic operates in real-time at the edge node using a sliding-window strategy without adding computational overhead. Through these optimizations in transmission strategy and fault tolerance, the system effectively reduces latency and network pressure while enhancing stability and reliability in complex environments. In the optimized data transmission and compensation stage, the Signal Magnitude Vector (SMV) is introduced to calculate the feature extraction of three-axis acceleration. The calculation is shown in equation (7) [18].

$$\mathrm{SMV}(t)=\sqrt{(a_x(t)-\bar{a}_x)^2+(a_y(t)-\bar{a}_y)^2+(a_z(t)-\bar{a}_z)^2} \tag{7}$$

In equation (7), $\bar{a}_x$, $\bar{a}_y$, and $\bar{a}_z$ respectively represent the sliding average of axial acceleration, which is used to eliminate long-term bias and enhance sensitivity and robustness to fall events. Meanwhile, to monitor heart rate abnormalities, Heart Rate Variability (HRV) is introduced as a feature, as shown in equation (8) [19].

$$\mathrm{HRV}=\sqrt{\frac{1}{N-1}\sum_{i=1}^{N}(RR_i-\overline{RR})^2} \tag{8}$$

In equation (8), RR_i represents the i-th heartbeat interval. $\overline{RR}$ represents the average interval between heartbeats. N represents the total number of heartbeats. HRV features are used together with SMV as inputs for fall detection and anomaly determination modules at edge nodes, ensuring the integrity of data transmission information. Based on the calculated SMV and HRV features, they can be further fed into the fall detection algorithm for classification. The overall process is shown in Figure 5.

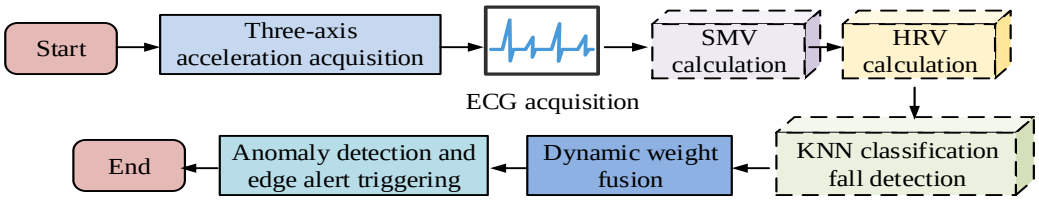

Figure 5: Fall detection algorithm flow

As shown in Figure 5, the fall detection algorithm process is designed based on multi-modal feature fusion. The algorithm first collects acceleration and heart rate signals through the terminal, and calculates synthetic motion features and HRV. Subsequently, the processed features are input into the classifier for fall detection, and the detection result triggers an abnormal alarm signal. Edge nodes decide whether to immediately report to the cloud for further analysis or cache locally for synchronization based on alarm priority. This algorithm improves the accuracy and robustness of fall event recognition by integrating motion and physiological signal features. In this process, the K-Nearest Neighbors (KNN) classifier is employed at the edge node for multi-modal feature classification. Compared with deep or kernel-based methods that require extensive parameter training and structural optimization, KNN offers low computational cost, no need for model pretraining, and easy deployment on resource-constrained devices. It ensures reliable classification accuracy while significantly reducing latency and energy consumption, aligning well with the real-time requirements of the proposed cloud-edge-end collaborative architecture. The specific implementation method is shown in equation (9) [20].

$$y=\arg\max_{c\in C}\sum_{i\in K}w_i\cdot\theta(y_i=c) \tag{9}$$

In equation (9), C represents the set of categories. K represents the set of nearest neighbor samples. w_i represents the weight of each neighbor. θ represents the indicator function. y_i represents the category of neighbors. To quantify the optimization effect of WiFi transmission, the system evaluates the link quality through a Packet Loss Rate (PLR), as shown in equation (10).

$$P_{loss}=\frac{N_{lost}}{N_{total}} \tag{10}$$

In equation (10), N_{lost} represents the number of lost packets. N_{total} represents the total number of data packets sent. P_{loss} represents the PLR. While optimizing transmission efficiency, the data compression ratio is used to measure the compression effect, as shown in equation (11).

$$R_{comp} = \frac{S_{original} - S_{compressed}}{S_{original}} \quad (11)$$

In equation (11), $S_{original}$ represents the size of the original data. $S_{compressed}$ represents the compressed data size. R_{comp} represents the compression ratio. The improved compression ratio not only reduces the network load, but also reduces the terminal energy consumption, providing more efficient data support for subsequent edge computing and cloud analysis. The multi-modal features are fused at the edge node to form the final decision output, and the weight fusion is shown in equation (12).

$$V_{fused} = \beta \cdot V_{SMV} + (1-\beta) \cdot V_{HRV} \quad (12)$$

In equation (12), V_{SMV} represents the motion feature value. V_{HRV} represents the HRV feature value. β represents the weight adjustment coefficient. V_{fused} represents the output after fusion. When designing the multi-modal fusion module, a linear weighted model is selected due to its simplicity, interpretability, and low computational cost, making it well suited for real-time inference on wearable and edge devices. Compared with more complex fusion strategies such as attention mechanisms or ensemble learning, the linear model offers higher energy efficiency and easier deployment without additional training or memory overhead. Subsequent experimental results further demonstrate that this choice provides a balanced trade-off between detection accuracy and latency. After calculating the weight fusion of each algorithm, the system integrates multi-modal features with optimization strategies to form a complete monitoring process, as shown in Figure 6.

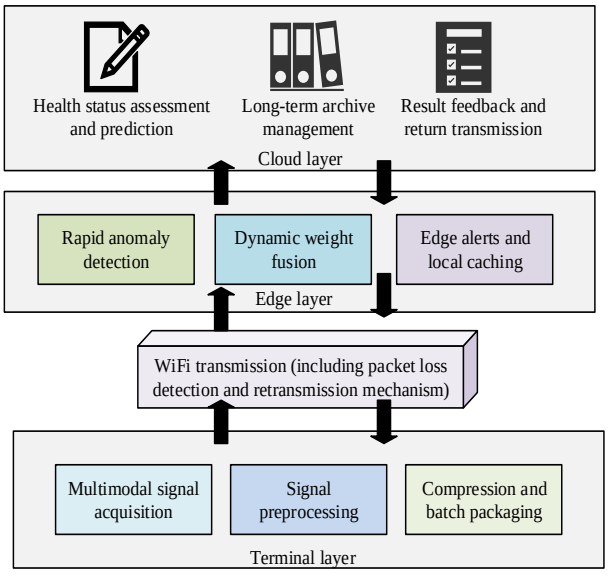

Figure 6: Optimized complete system workflow

As shown in Figure 6, the optimized complete system workflow integrates the end, edge, and cloud layers together with various optimization strategies. Firstly, the terminal performs multi-modal data acquisition and preprocessing, extracting key physiological and environmental features. The MCU then segments the data, appends timestamps, and transmits it through the optimized WiFi process while applying packet loss compensation, data compression, and batch transmission mechanisms. The edge node conducts rapid anomaly detection and performs multi-path fusion-based consistency analysis to handle potential signal conflicts. When discrepancies arise between different modalities (e.g., physiological and motion features), the system re-evaluates them based on confidence levels and temporal variation trends. If conflicting signals persist and the overall anomaly confidence increases, a prioritized alert is triggered and forwarded to the cloud for further verification. If the inconsistency is identified as transient noise or posture variation, the alert is temporarily suppressed to avoid false alarms. Finally, the cloud performs deep fusion analysis and health status evaluation, returning monitoring results and alerts to the terminal to achieve a closed-loop monitoring process. This workflow demonstrates the comprehensive optimization of the system in multi-mode conflict handling, low latency, high reliability, and high accuracy. To clarify the computational responsibilities across different layers, the proposed system defines a clear split between the terminal, edge, and cloud components. The terminal layer handles multi-modal data acquisition and basic preprocessing, including ECG filtering, motion sensing, and RSSI monitoring. The edge layer performs HRV feature computation, feature normalization, and KNN-based anomaly detection for real-time response. The cloud layer manages large-scale data fusion, model training, and adaptive system optimization. The functional division of tasks is summarized in Table 1.

Table 1: Functional division of tasks across terminal, edge, and cloud layers

Layer	Main tasks	Module	Output
End	Data acquisition & preprocessing	AD8232 ECG, MPU-6050 motion sensing, RSSI monitoring	Filtered signals, motion data
Edge	Feature computation & local classification	HRV calculation, feature normalization, KNN classifier	Real-time alerts
Cloud	Global analysis & adaptive optimization	Deep fusion model training, user profiling, system tuning	Long-term assessment & model updates

3 Results and analysis

3.1 Hyperparameter selection and performance ablation testing for wearable monitoring systems

During the experimental phase, a hardware and software operating environment suitable for joint monitoring of wearable devices and WiFi communication is established. The CPU is Intel Xeon Gold 6338, the GPU is NVIDIA RTX A6000 48GB, and the motherboard supports Gigabit Ethernet and WiFi 6 wireless networks, ensuring high-speed data exchange between the end, edge, and cloud. The software runs on the Ubuntu 20.04 LTS operating system, with Python 3.10 and TensorFlow 2.12 deep learning frameworks deployed on edge nodes. A Flask-based data interface is configured in the cloud to collect, transmit, analyze, and store monitoring data. In addition, the wearable terminal incorporates an AD8232 analog front-end ECG module for 0.5-50 Hz cardiac signal acquisition and an MPU-6050 accelerometer-gyroscope sensor for motion and posture tracking. Wireless communication relies on ESP32 microcontrollers that support WiFi 6. The WiFi signal quality is evaluated using the Received Signal Strength Indicator (RSSI), with a time-weighted averaging scheme applied to smooth instantaneous fluctuations and reflect link stability under varying interference conditions. The power consumption model is derived from each module's rated power and duty cycle, with total energy consumption expressed in milliwatts (mW) to evaluate energy distribution and efficiency under different operational states.

To verify the performance of the system in fall detection, health status recognition, and multi-modal fusion judgment, the study selects the SisFall Falls and Daily Activities Dataset (SisFall) and the MIT-BIH Physiological Signal Database (MIT-BIH) as the test datasets. The SisFall Dataset and the MIT-BIH Database are selected as the testing datasets. The SisFall dataset, jointly developed by Universidad de los Andes (Colombia) and Universidad Técnica Federico Santa María (Chile), contains tri-axial acceleration and angular velocity data collected from subjects wearing accelerometers and gyroscopes performing 15 fall scenarios and 19 daily activities. The participants are mainly middle-aged and elderly, providing representative motion features and activity patterns suitable for validating wearable fall detection algorithms. The MIT-BIH database includes ECG, blood pressure, and various physiological signals from participants across different age ranges. It has been widely used for HRV analysis and arrhythmia detection, supporting the evaluation of system stability and generalization under diverse physiological conditions. During data preprocessing, ECG signals are filtered using a 0.5-50 Hz bandpass filter to remove baseline drift and high-frequency noise. The sampling rate is unified at 360 Hz, and HRV features are extracted using a 10-second sliding window with 50% overlap. The tri-axial acceleration signals in the SisFall dataset are sampled at 200 Hz and processed through normalization and temporal alignment to ensure consistency across subjects and synchronization with ECG data. To determine the optimal performance parameter configuration for each module in the system, a hyperparameter selection test is conducted on the warning threshold adjustment coefficient α and weight adjustment coefficient β. The test results are shown in Figure 7.

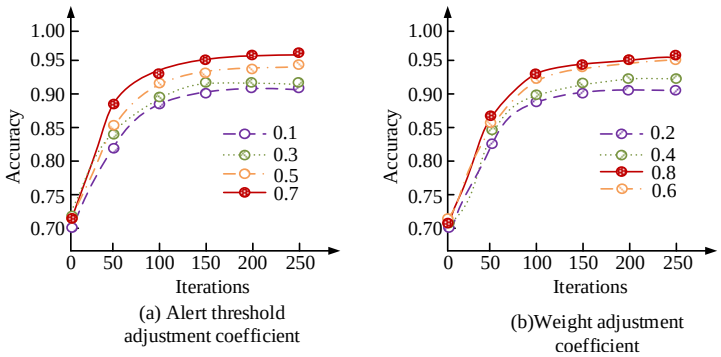

(a) Alert threshold adjustment coefficient

(b)Weight adjustment coefficient

Figure 7: Hyperparameter test results

Figure 7 (a) shows the results of the selection test for the warning threshold adjustment coefficient α, and Figure 7 (b) shows the results of the selection test for the weight adjustment coefficient β. As shown in Figure 7 (a), with the gradual increase of α, the overall accuracy of the system during the training process showed an upward trend. When α=0.7, the proposed system could quickly improve accuracy at multiple iteration points and reach the highest value of 96.4% when the iteration approached the stable stage. When α was set to 0.3 or below, the accuracy improvement was slow and the final level was low, indicating that a small threshold adjustment was not sufficient to effectively determine abnormal events. As shown in Figure 7 (b), with the increase of β, the accuracy of the system in multi-modal feature determination gradually improved. When β=0.6, the accuracy reached the highest 95.8%, indicating that the fusion weight allocation between motion features and HRV features was most reasonable at this time, which could fully utilize the complementary advantages of the two types of information and improve the recognition accuracy of falls and health abnormalities. Therefore, the study ultimately determined the optimal combination of hyperparameters as α=0.7 and β=0.6, under which the overall performance of the system was optimal. The study continues to conduct ablation tests on each module of the system on two datasets, and the results are shown in Figure 8.

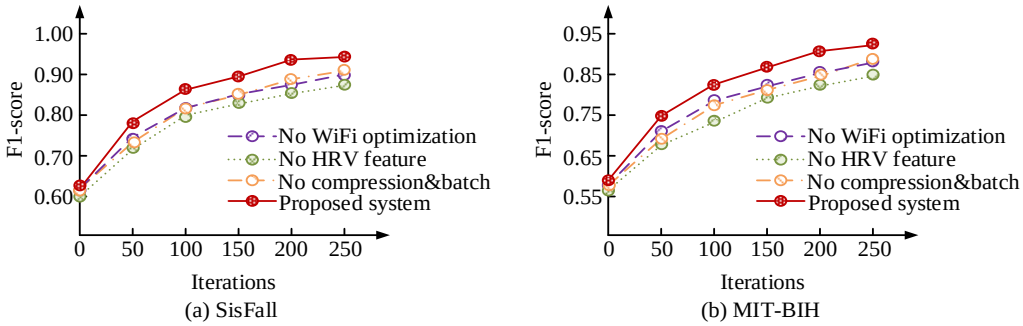

Figure 8: Ablation test results

Figure 8 (a) shows the ablation test results on the SisFall dataset, and Figure 8 (b) shows the results on the MIT-BIH dataset. According to Figure 8 (a), the F1-score of the complete system stabilized at 0.94 after 250 iterations. In contrast, after removing WiFi transmission optimization, the final F1-score was 0.90. After removing HRV features, it decreased to 0.88. After removing data compression and batch transmission, it was 0.91. Similarly, in Figure 8 (b), the F1-score of the complete system ultimately reached 0.92, higher than that of the other three baseline models. The ablation test results indicate that deleting all three modules will lead to a decrease in F1-score. The ECG scene is more sensitive to HRV features, and removing the HRV feature module has the greatest impact on the overall performance of the system. To evaluate the impact of each functional module on the overall system performance, comparative experiments were conducted on the SisFall and MIT-BIH datasets. The results are summarized in Table 2.

Table 2: Test results for different indicators on SisFall and MIT-BIH datasets

Data set	Method	Precision/%	Recall/%	Specificity/%
SisFall	No WiFi optimization	94.5	92.1	95.0
	No HRV feature	93.2	90.6	94.0
	No compression&batch	93.9	91.3	94.7
	Proposed system	97.0	95.4	97.6
MIT-BIH	No WiFi optimization	94.2	91.9	94.0
	No HRV feature	92.8	90.2	92.5
	No compression&batch	93.5	91.0	93.3
	Proposed system	96.1	94.8	96.3

According to Table 2, on the SisFall dataset, the precision of the complete system reached 97.0%, the recall rate was 95.4%, and the specificity was 97.6%. On the MIT-BIH dataset, the system also maintained a leading position with a precision of 97.6%, a recall rate of 94.8%, and a specificity of 96.3%. In contrast, the version without HRV features showed a significant decrease in recall rates on both datasets, at 90.6% and 90.2%, respectively, indicating that this feature played a crucial role in identifying falls and heart rate abnormalities. After removing WiFi optimization or data compression and batch transmission, although the three

indicators slightly decreased, the overall performance still exceeded 91%, verifying that the system had robustness.

3.2 Simulation testing of wearable monitoring system

To further verify the adaptability and stability of the proposed wearable elderly monitoring system under different practical scenarios, three types of simulation environments, including low, medium, and high interference, were constructed based on the SisFall and MIT-BIH real-world datasets, corresponding to daily home, outdoor, and complex field monitoring conditions. To create representative simulation environments, multiple interference factors were introduced into the original datasets, including sensor noise, motion artifacts, and WiFi link attenuation. Specifically, zero-mean Gaussian white noise was added to the acceleration and ECG signals to simulate sampling errors and ambient electromagnetic interference, while amplitude fluctuations and periodic disturbances were introduced to reproduce body motion and posture variations during device usage. In addition, the SNR and path loss exponent (n) were adjusted to emulate network instability during WiFi data transmission. To ensure reproducibility, the interference intensity was classified according to noise variance and SNR parameters: In the low-interference environment, the noise variance was set to 0.01 with SNR above 30 dB; In the medium-interference environment, the noise variance was 0.05 with SNR around 20 dB; In the high-interference environment, the noise variance was 0.1 with SNR reduced to 10 dB, accompanied by randomly injected motion artifact signals. These interferences were applied to the original samples through weighted addition during the data preprocessing stage to maintain the structural and temporal consistency of the signals.

In the testing, three widely used comparison systems are selected, namely the Hidden Markov Model-based Fall Detection (HMM-FD), Convolutional LSTM-based Wearable Monitoring (ConvLSTM-WM), and Graph Convolutional Network-based Pose Monitoring (GCN-Pose). The study uses sensitivity as an indicator to test the response capability of each system to abnormal events in three types of simulation environments. The test results are shown in Figure 9.

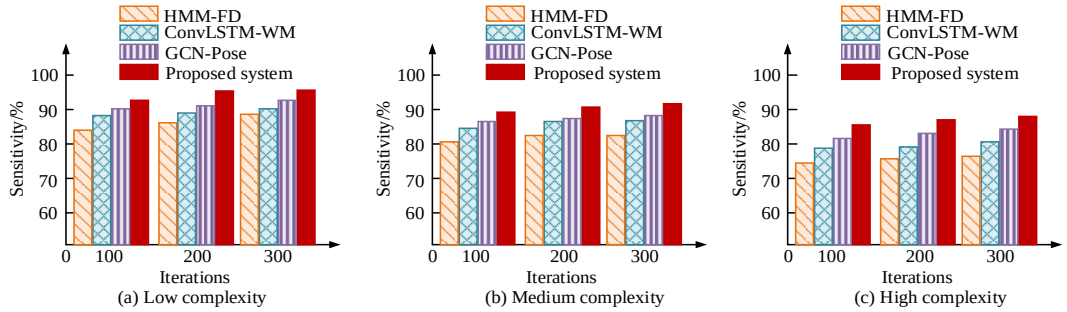

Figure 9: Sensitivity comparison of four wearable monitoring systems

Figures 9 (a), 9 (b), and 9 (c) respectively show the sensitivity changes of four systems in low, medium, and high complexity simulation environments. In Figure 9 (a), the proposed system increased from 92.8% to 94.8% in low complexity, which was 2.9%, 4.6%, and 7.7% higher than that of GCN-Pose, ConvLSTM-WM, and HMM-FD, respectively. At the medium complexity in Figure 9 (b), the sensitivity of the proposed system increased from 89.5% to 91.4%, while GCN-Pose, ConvLSTM-WM, and HMM-FD were 87.5%, 85.8%, and 82.3%, respectively. In the high complexity scenario shown in Figure 9 (c), the overall sensitivity of each system decreased, while the proposed system increased from 85.0% to 86.8%, still leading the three comparison systems. Overall, the proposed system maintains the highest sensitivity in each type of simulation environment, indicating that the system's ability to detect abnormal events is more robust in simulating real home interference and multi-action scenarios.

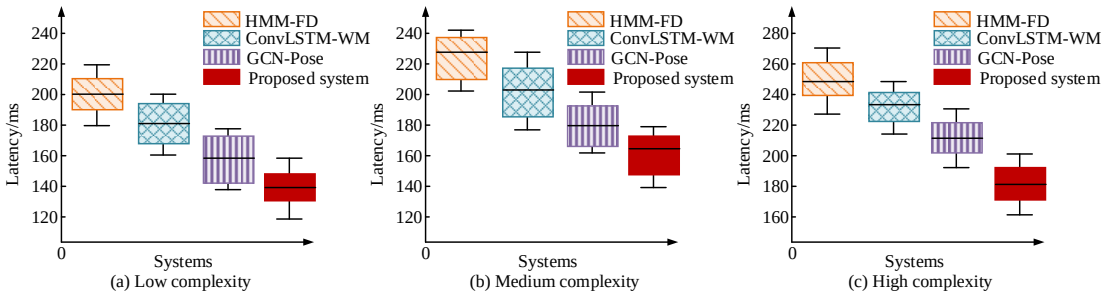

Figure 10: Event detection latency results

Figures 10 (a), 10 (b), and 10 (c) respectively show the test results of event detection latency box plots for four systems under three different levels of complexity. There were significant differences in latency among systems in low complexity, medium complexity, and high complexity environments. As shown in Figure 10 (a), in the low complexity, the latency of HMM-FD was relatively high, with a median of 200 milliseconds, while the median of the proposed system was only 140 milliseconds. From Figure 10 (b), in the medium complexity environment, the latency of all four systems increased, but the proposed system still maintained the lowest median latency of 160 milliseconds, which was better than that of other systems. In Figure 10 (c), high complexity testing resulted in HMM-FD latency reaching 250 milliseconds, while the median latency of the proposed system was 180 milliseconds, maintaining optimal performance. Overall, the proposed system exhibits low latency and high stability in all three types of simulation environments, proving its excellent event response capability and robustness under different levels of complexity and signal interference conditions. To clearly illustrate the overall performance of each monitoring system under different simulation environments, three key metrics, sensitivity, F1-score, and detection latency were summarized and compared. The results are shown in Table 3.

Table 3: Test results of classification performance under different conditions

Situation	Method	F1-score	Sensitivity/%	Latency /ms
Low complexity	HMM-FD	0.89	87.1	200
	ConvLSTM-WM	0.91	90.2	175
	GCN-Pose	0.92	91.9	165
	Proposed system	0.94	94.8	140
Medium complexity	HMM-FD	0.86	82.3	225
	ConvLSTM-WM	0.88	85.8	198
	GCN-Pose	0.89	87.5	188
	Proposed system	0.91	91.4	160
High complexity	HMM-FD	0.83	79.4	250
	ConvLSTM-WM	0.85	82.1	230
	GCN-Pose	0.86	83.6	215
	Proposed system	0.88	86.8	180

As shown in Table 3, the proposed system achieved F1-scores of 0.94, 0.91, and 0.88 under low, medium, and high interference environments, respectively, higher than that of HMM-FD, ConvLSTM-WM, and GCN-Pose, indicating superior detection accuracy and stability across different scenarios. Considering the overall performance in sensitivity and latency, the proposed system consistently balanced detection accuracy and response speed under varying complexity, demonstrating strong robustness and adaptability. Statistical significance analysis further confirmed that the improvements in F1-score (p=0.032) and detection latency (p=0.019) were significant at the α=0.05 level, indicating that the performance advantage was statistically meaningful rather than random variation.

The study continues to compare the test results of four models under three different operating conditions, including False Alarm Rate (FAR), Energy Consumption (EC), and PLR. When calculating EC, direct hardware measurements were not performed. On the contrary, these values were estimated based on the typical power consumption parameters of key wearable terminal components, including the MCU, sensors, and WiFi communication module. Specifically, the average power demand of each component was derived from its rated operating voltage and average current under different activity states, and the overall energy consumption was obtained by combining these values with the system's task execution time. All parameters were taken from publicly available component datasheets and experimental runtime logs, reliably estimating the system's energy consumption trends during the cloud-edge-end collaborative operation. The results are shown in Table 4.

Table 4: Test results under different conditions

Situation	Method	FAR%	EC/mW	PLR/%
Low complexity	HMM-FD	7.5	82.3	1.8
	ConvLSTM-WM	6.2	95.1	1.5
	GCN-Pose	5.5	110.4	1.2
	Proposed system	3.8	88.7	0.9
Medium complexity	HMM-FD	9.1	84.5	2.6
	ConvLSTM-WM	7.3	97.8	2.1
	GCN-Pose	6.5	112.0	1.8
	Proposed system	4.5	90.3	1.1
High complexity	HMM-FD	11.4	87.2	3.5
	ConvLSTM-WM	9.0	101.2	2.9
	GCN-Pose	7.8	115.5	2.3
	Proposed system	5.2	92.1	1.4

According to Table 4, in the low complexity environment, the HMM-FD system had the weakest performance with a FAR of 7.5%, EC of 82.3mW, and signal PLR of 1.8%. In contrast, the proposed system had a FAR of only 3.8%, EC of 88.7mW, and signal PLR of 0.9% in low complexity environments, demonstrating high efficiency and reliability. In the medium complexity environment, the performance gap between systems further widened, and the proposed system still maintained a low FAR of 4.5% in this environment. In the high complexity environment, the FARs of HMM-FD and ConvLSTM-WM increased to 11.4% and 9.0%, respectively, and the signal PLR increased significantly. The proposed system still maintained the lowest FAR of 5.2%, signal PLR of 1.4%, and EC of 92.1mW, proving that the system exhibited good comprehensive performance and strong robustness in accuracy, reliability, and EC control.

4 Discussion

4.1 Privacy and security considerations

Given that the proposed elderly monitoring system involves the acquisition and transmission of physiological and behavioral data, data privacy and security have been carefully considered in the system design. Communication between the end and edge nodes employs AES-256 encryption to prevent data interception or tampering during WiFi transmission. Cloud-side data storage and access are protected through user authentication and permission control to avoid unauthorized access. While the current study primarily focuses on monitoring and detection performance, future work will incorporate end-to-end encryption, data anonymization, and compliance with international privacy standards such as GDPR, further enhancing system reliability and security in healthcare applications.

4.2 System performance analysis and comparative discussion

This study develops a multi-mode monitoring system that integrates WiFi communication and wearable sensing, which solves the challenges of unstable signals, large movement changes, and latency in elderly health monitoring. The system is systematically validated on two public datasets, SisFall and MIT-BIH. The experimental results show that the proposed system outperforms HMM-FD, ConvLSTM-WM, and GCN-Pose in F1-score, sensitivity, and detection latency, demonstrating strong robustness and real-time responsiveness. The performance improvement mainly stems from three aspects. Firstly, the HRV analysis at the feature level allows the system to capture both motion and physiological anomalies, improving the accuracy of abnormal event detection. Secondly, the WiFi transmission optimization and compression-compensation mechanism effectively reduces data loss and latency, ensuring stability under complex interference conditions. Thirdly, the edge-cloud collaborative architecture with dynamic threshold adjustment achieves balanced computation and communication loads, enhancing performance under high concurrency.

Compared with existing approaches, HMM-FD relies on statistical modeling and struggles with multi-modal data. ConvLSTM-WM achieves strong temporal modeling but suffers from high computational cost and energy consumption. GCN-Pose performs well in pose estimation but is more sensitive to interference. In contrast, the proposed system jointly models physiological and motion features, achieving a superior trade-off between detection accuracy and power efficiency.

Nevertheless, certain limitations remain. The dynamic adjustment mechanism may increase energy consumption in multi-node scenarios, and system stability can still be affected by WiFi coverage and environmental occlusion. Future work will explore federated learning and adaptive energy management strategies to improve distributed performance, privacy protection, and long-term operational reliability.

5 Conclusions and recommendations

A monitoring system combining WiFi transmission optimization, HRV feature analysis, and multi-modal data fusion was proposed to address the data noise interference, motion complexity, and multi-modal feature fusion in fall detection and health status monitoring of wearable elderly monitoring systems. The system rapidly identified abnormal events by adjusting the warning threshold coefficient and optimizing the fusion weight, and combined the end-to-end cloud collaborative architecture to ensure efficient data transmission and processing. The hyperparameter tests on the SisFall and MIT-BIH real datasets showed that when the warning threshold adjustment coefficient was set to 0.7 and the fusion weight coefficient was 0.6, the system performance was optimal, with F1-scores reaching 0.94 and 0.92, respectively. In a simulation environment, the proposed system was compared with three typical monitoring systems. The sensitivity of the proposed system could reach up to 94.8% in low, medium, and high interference environments, with a minimum event detection latency of 140 milliseconds. The minimum FAR of the system was only 3.8%, and the signal PLR was 0.9%, fully reflecting its strong robustness and real-time response capability under complex actions and interference conditions.

In summary, the WiFi-based wearable monitoring scheme demonstrates unique advantages in non-contact sensing, low-power operation, and environmental adaptability. Compared with traditional systems that rely on single-sensor input or control-oriented feedback, it exhibits higher reliability and deployment flexibility. Future research may further integrate artificial intelligence techniques to enable health risk prediction and trend analysis, utilizing temporal deep learning and graph neural network models to enhance health status assessment and early warning capabilities. In addition, research focused on battery optimization, multi-node collaborative scalability, and user-friendly interaction design can further promote the long-term application and large-scale deployment of wearable monitoring systems in intelligent elderly care and home healthcare scenarios.

References

[1] Chen C, Ding S, Wang J. Digital health for aging populations. Nature medicine, 2023, 29(7): 1623-1630. DOI: 10.1038/s41591-023-02391-8.

[2] Ledesma J R, Ma J, Zhang M. Global, regional, and national age-specific progress towards the 2020 milestones of the WHO End TB Strategy: a systematic analysis for the Global Burden of Disease Study 2021. The Lancet infectious diseases, 2024, 24(7): 698-725. DOI: 10.1016/S1473-3099(24)00007-0.

[3] Naeini E K, Sarhaddi F, Azimi I. A deep learning–based PPG quality assessment approach for heart rate and heart rate variability. ACM Transactions on Computing for Healthcare, 2023, 4(4): 1-22. DOI: 10.1145/3616019

[4] Babu M, Lautman Z, Lin X. Wearable devices: implications for precision medicine and the future of health care. Annual review of medicine, 2024, 75(1): 401-415.DOI: 10.1146/annurev-med-052422-020437.

[5] Dewangan L, Vaishnava A R. Energy-efficient smart wearable IoT device for the application of collapse motion detection and alert. IETE Journal of Research, 2023, 69(2): 1133-1139. DOI: 10.1080/03772063.2020.1859952.

[6] Tan L, Yu K, Bashir A K, Cheng X, Ming F, Zhao L, Zhou X. Toward real-time and efficient cardiovascular monitoring for COVID-19 patients by 5G-enabled wearable medical devices: A deep learning approach. Neural Computing and Applications, 2023, 35(19): 13921-13934. DOI: 10.1007/s00521-021-06219-9.

[7] Chen J, Wang W, Fang B, Liu Y, Yu K, Leung V C M. Digital twin empowered wireless healthcare monitoring for smart home. IEEE Journal on Selected Areas in Communications, 2023, 41(11): 3662-3676. DOI: 10.1109/JSAC.2023.3310097.

[8] He J, Zhu W, Qiu L, Zhang Q, Wang C. An indoor fall detection system based on WiFi signals and genetic algorithm optimized random forest. Wireless Networks, 2024, 30(3): 1753-1771. DOI: 10.1007/s11276-023-03625-w.

[9] Ghoshal S, Saif S, Biswas S. Optimizing Indoor Positioning: ANN-GD Fusion for Enhanced Accuracy in WiFi Fingerprint-Based Surveillance Systems. SN Computer Science, 2025, 6(5): 511-512. DOI: 10.1007/s42979-025-04029-7.

[10] Zhang X, Gu Y, Yan H, Wang Y, Dong M, Ota K. Wital: A COTS WiFi devices based vital signs monitoring system using NLOS sensing model. IEEE Transactions on Human-Machine Systems, 2023, 53(3): 629-641. DOI: 10.1109/THMS.2023.3264247.

[11] Sirtoli V G, Liamini M, Lins L T. Removal of motion artifacts in capacitive electrocardiogram acquisition: A review. IEEE Transactions on Biomedical Circuits and Systems, 2023, 17(3): 394-412. DOI: 10.1109/TBCAS.2023.3270661.

[12] Ghasemi S, Sotoudeh B, Pazhooh M. Design and simulation of a novel MEMS-based single proof mass three-axis piezo-capacitive accelerometer. Microsystem Technologies, 2024, 30(3): 279-289. DOI: 10.1007/s00542-023-05604-9.

[13] Bellier P, Coppieters’t Wallant D, van den Bongarth H. A wireless low-power single-unit wearable system for continuous early warning score calculation. IEEE Sensors Journal, 2023, 23(11): 12171-12180. DOI: 10.1109/JSEN.2023.3267146.

[14] Gupta V. DBPF pre-processing-based improved ECG signal analysis in medical engineering applications. International Journal of Engineering Systems Modelling and Simulation, 2025, 16(2): 111-118. DOI: 10.1504/IJESMS.2025.144881.

[15] Lv Z, Singh A K. Edge-cloud-based wearable computing for automation empowered virtual rehabilitation. IEEE Transactions on Automation

Science and Engineering, 2023, 21(3): 3896-3909. DOI: 10.1109/TASE.2023.3289908.

[16] Reaño C, Riera J V, Romero V. A cloud-edge computing architecture for monitoring protective equipment. Journal of cloud computing, 2024, 13(1): 82-83. DOI: 10.1186/s13677-024-00649-1.

[17] Boulkroune A, Zouari F, Boubellouta A. Adaptive fuzzy control for practical fixed-time synchronization of fractional-order chaotic systems. Journal of Vibration and Control, 2025: 10775463251320258.

[18] Renteria-Pinon M, Tang X, Tang W. Real-time in-sensor slope level-crossing sampling for key sampling points selection for wearable and iot devices. IEEE Sensors Journal, 2023, 23(6): 6233-6242. DOI: 10.1109/JSEN.2023.3243460.

[19] Lin I M, Chen T C, Tsai H Y. Four sessions of combining wearable devices and heart rate variability (HRV) biofeedback are needed to increase HRV indices and decrease breathing rates. Applied psychophysiology and biofeedback, 2023, 48(1): 83-95. DOI: 10.1007/s10484-022-09567-x.

[20] Kausar F, Mesbah M, Iqbal W. Fall detection in the elderly using different machine learning algorithms with optimal window size. Mobile Networks and Applications, 2024, 29(2): 413-423. DOI: 10.1007/s11036-023-02215-6.